DOI: 10.26599/FSHW.2026.9250926

Y. Xia et al. / Food Science and Human Wellness 16 (2027)

Contents lists available at SciOpen

Food Science and Human Wellness

journal homepage: https://www.sciopen.com/journal/2097-0765

China Food Publishing Co.

Chlorogenic acid inhibits smooth muscle cell senescence and phenotypic switch to alleviate aortic dissection

Yi Xia[#1], Huan Tang[#2], Zhixi Wei[1], Wenting Zhao[1], Wenhua Jin[1], Hejing Tang[1], Chang Fan[1], Sitong Wan[1], Senyang Hu[1], Peng An[1], Junjie Luo*[1], Yongting Luo*[1], Yinhua Zhu*[1]

[1]*Department of Nutrition and Health, China Agricultural University, Beijing, 100193, China*

[2]*State Key Laboratory for Quality Ensurance and Sustainable Use of Dao-di Herbs, Artemisinin Research Center, and Institute of Chinese Materia Medica, China Academy of Chinese Medical Sciences, Beijing, China*

ABSTRACT: Cellular senescence and inflammation-mediated phenotypic switch in smooth muscle cell (SMC) are pivotal factors in the development of aortic dissection. Chlorogenic acid (CGA), a polyphenolic compound of plant origin, exhibits remarkable anti-aging and anti-inflammation properties. However, the role of CGA in aortic dissection remains elusive. In this study, a β-aminopropionitrile (BAPN)-induced aortic dissection model *in vivo* and DOX-induced cell senescence model *in vitro* were employed, in combination with activity-based protein profiling (ABPP) technology, to explore the target by which CGA inhibits aortic dissection. The results revealed that CGA could prophylactically and therapeutically prevent BAPN-induced aortic dissection in mice. Transcriptome sequencing of aortic tissues demonstrated that CGA treatment downregulated the expression of genes related to senescence and synthesis, while upregulating the expression of contractile genes. These findings were further validated in DOX-induced senescent SMCs. Based on ABPP technology, a CGA chemical probe was utilized to explore its protein targets, and Mettl3 was identified and verified as a potential target of CGA in senescent SMCs. Our study offers novel insights into halting the progression of aortic dissection and may facilitate the application of CGA in the prevention of aortic dissection.

Key words: aortic dissection, chlorogenic acid, smooth muscle cell, cell senescence, phenotypic transformation

1. Background

Aortic dissection (AD) represents a life-threatening disorder, characterized by an intimal tear that precipitates the separation of the aortic wall and the formation of a false lumen [1–3]. The cardinal pathological features of AD encompass the phenotypic switch of smooth muscle cells (SMCs) and the degradation of extracellular matrix [4]. Multiple risk factors contribute to the development of AD. Environmental factors, including smoking and alcohol consumption, in concert with genetic factors such as mutations in *Acta2* and *Myh11*, can increase the incidence of AD [5,6]. The incidence of AD peaks between the ages of 60 - 70 years [7]. Significantly, AD is associated with an alarmingly high mortality rate. Up to 50%

[#]These authors contributed equally to this work.
***Corresponding author**
zhuyinhua@cau.edu.cn (Y. Zhu), luo.yongting@cau.edu.cn (Y. Luo), luojj@cau.edu.cn (J. Luo)

Received 5 March 2025
Received in revised from 30 April 2025
Accepted 28 September 2025

of patients succumb within two days, and this proportion escalates to 70% within one week. Currently, surgical repair, which involves repairing or replacing the damaged aorta, is the standard treatment modality. Additionally, medications such as β - blockers and vasodilators are administrated to mitigate the force of blood ejection [8]. However, despite its severity, the management of AD is hampered by a significant shortcoming：the conspicuous absence of screening and preventive management strategies.

Recent investigations have underscored the predominant role of SMCs in AD [9]. SMCs are fundamental to maintain morphology and elasticity of blood vessels. Single-cell RNA sequencing analysis has identified SMCs as a dynamic population endowed with remarkable phenotypic plasticity [10]. External stimulus drive SMCs to relinquish their contractile phenotype and gain other phenotypes [11]. Notably, inflammation-mediated phenotypic transformation has been found to significantly contribute to the onset of AD [12]. *TNF-α* has been demonstrated to induce the phenotypic switch of SMCs from the contractile to the synthetic phenotype [13,14]. Synthetic SMCs reduce the production of extracellular matrix components, such as collagen and elastin, which are crucial for maintaining the integrity of the aortic wall [15]. Additionally, aging is considered as a potential risk factor in AD [16]. Clinical statistics indicate that the elderly exhibit a higher AD morbidity compared to the young [17]. The number of senescent vascular SMCs (VSMCs) is remarkably increased in the aortic walls of elderly AD patients relative to younger counterparts. Senescent VSMCs lose their normal contractile function and acquire a senescence-associated secretory phenotype (SASP) [18]. For example, miR-1204 directly targets *myosin light chain kinase* (*MYLK*) gene, leading to VSMC senescence, the acquisition of SASP, and the loss of their contractile phenotype, thereby exacerbating the pathological process of AD [19]. Collectively, the evidence suggests that intervening SMC senescence and phenotypic switch may be an effective measure to impede the progression of AD.

Chlorogenic acid (CGA), a polyphenolic compound, is widely distributed in coffee beans, fruits such as apples, pears, as well as vegetables like potatoes and spinach. It is also present in various herbs and medicinal plants [20]. Numerous studies have identified the remarkable anti-inflammatory and antioxidant properties of CGA. In terms of its anti-inflammatory effects, CGA can modulate inflammatory mediators [21]. For instance, it has been found to upregulate the expression of anti-inflammatory cytokines like *interleukin-4* (*Il-4*) and *interleukin-10* (*Il-10*), while simultaneously downregulating the levels of pro-inflammatory cytokines such as *interleukin-1β* (*Il-1β*) and *interleukin-6* (*Il-6*). Additionally, recent research has revealed that CGA can significantly inhibit ultraviolet-induced skin cell senescence and reduce inflammation levels [22]. Thus, CGA may be a potential intervention drug for AD.

To examine whether CGA inhibited the progression of AD, we established a BAPN-induced AD model in mice. Both prophylactic and therapeutic administration of CGA demonstrated significant efficacy in suppressing AD progression in the model.. Subsequently, the mechanism by which CGA prevents AD was explored. The results demonstrated CGA down-regulated the SMC senescence and phenotypic transformation pathways in AD. This conclusion was also confirmed by a doxorubicin (DOX)-induced senescent model *in vitro*. Furthermore, a CGA probe was constructed to identify Mettl3 as the downstream target of CGA using

activity-based protein profiling (ABPP) technology, and inhibition of Mettl3 reduced the senescence and phenotypic transformation of SMCs *in vitro*. *In vivo*, STM2457 (Mettl3 inhibitor) was injected to the mice to certify the effect of Mettl3. Combined with the existing studies[23], activator protein-1 (AP-1) was considered as the potential downstream target of Mettl3. Then western blotting showed the reduction of JUN (AP-1 transcription factor subunit) on senescent MOVAs stimulated with STM2457 (Mettl3 inhibitor). In addition, the AP-1 inhibitor-T5224 effectively inhibits phenotypic transformation and senescence in DOX induced MOVAs.

2. Materials and methods

2.1 Regents

BAPN (β-aminopropionitrile monofumarate, HY-107829), CGA (chlorogenic acid, purity ≥99%, HY-N0055) and STM2457 (Mettl3 inhibitor, purity ≥99%, HY-134836) were purchased from MCE, China. The 4% BAPN feed was customized by HFK Bio Technology, Beijing. CGA-p (CGA-probe) was synthesized and validated as previously described [22]. Other reagents include TRIzol (15596026, Thermo, USA), Reverse Transcription Reagent kits (FT301, Vazyme, China), SYBR Green PCR mix (Q711-02, Vazyme, China), Masson's trichrome staining kit (G1340, Solarbio, China), Alcian blue (G1560, Solarbio, China), and Verhoeff Van Gieson elastin stain kit (ml093362, Mlbio, China).

2.2 Mouse experiments

Animal experiments were performed with the guidelines for the care and use of laboratory animals and were approved by the ethics committee of the China Agricultural University (the license approval number: AW02105202-5-2). C57BL/6J male mice (3 weeks old) were purchased from the Si Pei Fu Biotechnology, Beijing. Mice were maintained in standard conditions.

In experiment of CGA prophylactical intervention, 48 mice were randomly divided into 4 groups with each group of 12 mice, including control group BAPN group, CGA low dose group (CGA-L), and CGA high dose group (CGA-H). AD model was induced by 4% BAPN feed in mice. Mice of the control group were fed with normal feed and water. Other 3 groups of mice were fed with 4% BAPN feed, while the CGA low/high dose group of mice were intragastric administration with CGA 30/150 mg/kg/d. CGA was dissolved in DMSO and diluted with distilled water. All mice were sacrificed at day 21 (n = 48).

To evaluate the therapeuticeffect of CGA, we conducted therapeutic intervention model in mice. During the experiment, 48 mice were randomly divided into 4 groups with each group of 12 mice, including control group, BAPN group, Day14 group, and CGA group. Mice of the control group were fed with normal feed and water (n = 12). Other 3 groups of mice were fed with 4% BAPN feed. The CGA group of mice were intragastric administration with CGA 150 mg/kg/d when the first mouse died for AD. In this experiment, the first mouse died for AD at day 14. One group fed with 4% BAPN feed were evaluated with ultrasound, then sacrificed at day 14 (n = 12). The rest of mice were sacrificed at day 21 (n = 36).

STM2457, the inhibitor of Mettl3, was used to verify the effect of Mettl3 as downstream target of CGA in AD mouse model. 36 mice were randomly divided into 3 groups: control group, BAPN group, and STM2457 treated group. Control and BAPN group were treated as above. The mice in STM2457 group were intraperitoneally injected STM2457 was purchased from Bidepharm (BD01398922, China). The drug was dissolved in DMSO, and diluted with PEG400 (P8530, Solarbio, China), daily injected to mice at a dose of 30 mg/(kg.d) beginning with the death of first mouse in BAPN group. All mice were evaluated with ultrasound, then sacrificed at day 21.

2.3 Ultrasound imaging

The maximal diameter of ascending aorta was measured *in vivo* on day 21 using the Vevo 2100 High-Resolution Imaging System (FUJIFILM VisualSonics, Toronto, Canada) equipped with an 18-38 mhz scanning head (MS400, mouse cardiovascular). The mice were anesthetized with 1.5% vaporized isoflurane. Then, the mice were depilated on their chest and abdomen, and placed on their back on a thermostatic plate. Maintaining heart rate of the mice on 450-500 beats per minute (bpm), the maximal internal diameters of ascending aorta were measured at the level of the aortic outflow tract of innominate artery at end-diastole using the left ventricular long-axis view. All the results were recorded by one expert, and the measurements were taken by another experimenter.

2.4 Histological analyses

The mice were euthanized, perfused with PBS, and the aortas were exposed and excised. The tissues were placed into 4% PFA solution. The aortas were embedded and sectioned (5 μm thickness). Then, the slides were stained with Masson, Alcian blue and modified Verhoeff Van Gieson elastin (EVG) staining to reveal collagen fibers, proteoglycan deposition and the elastic fibers. Images were acquired using a Leica DM6B microscope with 20× or 40× HCPLAN objective lenses and Leica Application Suite 4.10 acquisition software and processed for presentation with Photoshop and Illustrator (Adobe, USA). Collagen and proteoglycan quantification were performed using ImageJ. Elastin breaks were counted in the medial layer. Each group used 4 mice, two sections per mouse.

2.5 RNA sequencing (RNA-seq)

Total RNA of aorta from the mice with control, BAPN and CGA low dose intervention group were subjected to bulk RNA-seq conducted by Metware (Wuhan, China).

Detailed information of library construction and data analysis was described previously [23]. A Kyoto encyclopedia of genes and genomes (KEGG) enrichment histogram of differential gene was illustrated with the q-value in the enrichment analysis results by selecting the KEGG pathways related to senescence and phenotypic transformation. And the column chart of enrichment items was drawn.

Volcanic maps were used to show the distribution of differential genes involving in senescence and phenotypic transformation. To screen differential gene, DESeq2 was used to conduct differential expression analysis among sample groups, and the differentially expressed gene sets between the two biological

conditions were obtained. Unstandardized reads count data of input genes are required, rather than standardized data such as RPKM and FPKM. The count of reads of genes is achieved using featureCounts. After the difference analysis, Benjamini-Hochberg method is also needed to perform multiple hypothesis testing correction for hypothesis testing probability (p-value) and obtain False Discovery Rate (FDR). The screening criteria for differential genes were |log2Fold Change| >= 1, and FDR < 0.05.

Differential expression cluster analysis was used to determine the expression patterns of differential genes under BAPN or CGA-induced conditions. The differential genes were standardized by Z-score, and the cluster heat map of all comparison groups was drawn. Senescence markers (such as *p16, Rbl1* and *Tnf-α*), contractile markers (such as *Tagln, Acta2* and *Pln*) and synthetic markers (such as *Mmp25, Ccl5* and *Col2a1*) were utilized to define different cell phenotypes.

2.6 Cell culture and treatment

Mouse aortic vascular smooth cell (MOVA) was obtained from ATCC (CRL-2797, USA), and cultured in Dulbecco's modified eagle medium (DMEM, C009, EallBio, China) supplemented with 10% fetal bovine serum (FBS), 1% penicillin/streptomycin. All cultures were maintained in a 37℃, 5% CO_2 cell incubator. The cells were washed with PBS, trypsinized, counted, and plated in 6/12-well plates depending on the experiments. MOVAs were treated with 200 nmol/L DOX to induce cell senescence and phenotypic switch.

In the prophylactic intervention model, 20 μmol/L CGA were added into medium with 200 nmol/L DOX for 48 h. In the therapeutic intervention model, after treating with 200 nmol/L DOX for 24 h, 20 μmol/L CGA were added into medium containing DOX for another 24 h. To detect the effect of CGA-analogue (CGA-A) *in vitro*, MOVAs were treated with 200 nmol/L DOX and 20 μmol/L CGA/CGA-A for 48 h. STM2457 was used to inhibit the expression of Mettl3. MOVAs treated with 200 nmol/L DOX were stimulated with 5 μmol/L STM2457 for 48 h simultaneously. Cells were collected for subsequent experimental studies.

2.7 Senescence-associated β-galactosidase (SA-β-gal) staining

SA-β-gal activity was determined using a SA-β-gal Staining Kit (Cat. No. C0602, Beyotime Biotechnology) as previously reported [24]. MOVAs were plated into 12-well plates. After treatments, the cells were removed medium and washed with PBS for 3 times. Then, the cells were fixed with paraformaldehyde for 15 min at room temperature. Subsequently, the cells were washed with PBS for 2 times, incubating with staining solution at 37℃ overnight. Finally, the cells were imaged with Leica microscope and the ratio of positive stained cells were calculated.

2.8 RNA isolation and quantitative PCR (qPCR)

Total RNA from mice aortic tissues and treated cells were extracted using TRIzol. The concentration of RNA was measured by NanoDrop OneC (Thermo Fisher Scientific, USA). Total RNA was reverse-transcribed into cDNA using Reverse Transcription Reagent kits. qPCR was executed using SYBR Green PCR mix on QuantStudio5 384-Well Block (Thermo Fisher Scientific, USA). All samples were

amplified using 6 biological replicates per sample. *β-actin* as the internal parameter. Results were analyzed using the comparative CT method. Sequences of primers used in this article are listed in Table S1.

2.9 Western blotting (WB)

Samples of treated-cell were collected, and lysed by lysis buffer (P0013, Beyotime). 10% SDS-PAGE were used to separate the proteins that transferred to PVDF membranes. Primary antibodies of target proteins and secondary antibodies were incubated to PVDF membranes. The proteins were visualized by Chemiscope 6100, and quantified with Image J.

2.10 CGA probe (CGA-p) synthesis

The synthesis of title compound involved one step. It was completed using a synthetic method as follows.

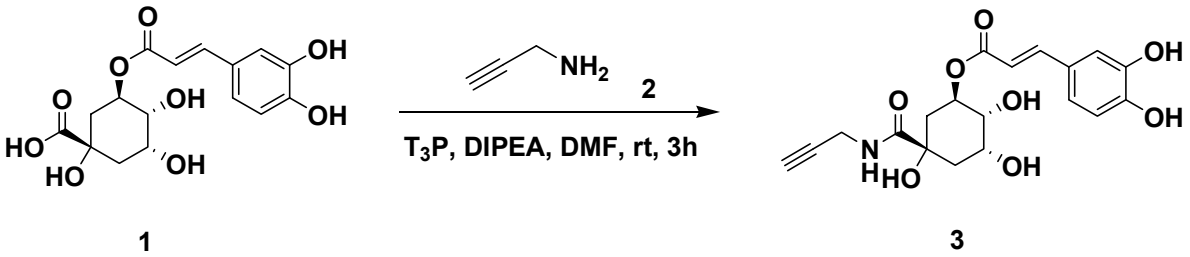

Scheme 1

According to the client's require, 60 mg of target compound was finally obtained, and confirmed by LCMS and 1H NMR.

To a solution of SM1 (500 mg, 1.41 mmol) and SM2 (233 mg, 4.24 mmol) in DMF (10 mL) was added DIPEA (547 mg, 4.24 mmol) and T3P (4.5 g, 7.05 mmol, 50% in EtOAc). The mixture was stirred at rt for overnight, then diluted with H_2O (20 mL) and extracted with EtOAc (20 mL*3), combined the organic phase and evaporated the solvent, the residue was purified by prep-HPLC to afford the desired product (60 mg, 11%) as a white solid.

MS: m/e =392(M+H)+. 1H NMR (400 MHz, DMSO) δ 8.16 (t, J = 5.9 Hz, 1H), 7.47 (d, J = 15.9 Hz, 1H), 7.04 (d, J = 1.8 Hz, 1H), 7.00 (dd, J = 8.2, 1.9 Hz, 1H), 6.76 (d, J = 8.1 Hz, 1H), 6.23 (d, J = 15.9 Hz, 1H), 5.59 (s, 1H), 5.23 (td, J = 10.4, 5.3 Hz, 1H), 4.09 (d, J = 2.9 Hz, 1H), 3.82 (dd, J = 5.9, 2.4 Hz, 2H), 3.58 (dd, J = 9.6, 2.7 Hz, 1H), 3.02 (d, J = 4.8 Hz, 1H), 2.00 – 1.81 (m, 3H), 1.75 (d, J = 14.2 Hz, 1H), 1.54 (d, J = 0.5 Hz, 1H), 0.95 (t, J = 7.1 Hz, 1H).

2.11 ABPP technology

2.11.1 ABPP technology to identify the protein targets of CGA in senescent SMCs

For in situ fluorescence labeling experiments, MOVAs were seeded in 6-well plates at a density of 5.0 × 10^5 cells/well for 24 h. CGA-p (1-50 μmol/L) or DMSO was added to the plates for 4 h. Next, the cells were washed three times with PBS to remove the residual drug probes. The harvested cells were lysed with the lysis buffer (0.1% Triton X-100 and 1% protease inhibitor). Soluble proteins were then obtained by centrifugation and protein concentration was determined by BCA assay (Pierce BCA protein assay kit). Subsequently, 100 μL of proteins (2 mg/mL) were taken from each group for the click chemistry reaction. The pre-mixed click

reaction reagents including 9 μL of TBTA (10 mmol/L in DMSO), 3 μL of TCEP (50 mmol/L in ddH_2O), 3 μL of $CuSO_4$ (50 mmol/L in ddH_2O), and 1 μL of TAMRA-azide (10 mmol/L in DMSO) were added into the lysate samples, and the reaction was conducted in a shaker with 800 r/min at 25℃ for 2 h. The proteins were precipitated using 1 mL of pre-chilled acetone at -20℃ for 30 min and purified by centrifugation. The samples were then dissolved in 50 μL of 1× loading buffer and then denatured for 5 min at 95℃ followed by separation in 12% SDS-PAGE gels. Finally, the labeling proteins were fluorescently imaged by a laser scanner (Azure Sapphire RGBNIR, USA) and stained with coomassie brilliant blue (CBB).

For in situ fluorescent labeling competition experiments, MOVAs were initially pretreated with CGA for 4 h and then incubated with CGA-p for another 4 h. Protein extraction, click chemical reaction and electrophoretic separation were performed as described above. For fluorescence labeling of recombinant protein, the protein was pretreated with or without different concentrations of CGA in PBS with vigorous shaking at 37℃ for 1 h, followed by probe treatment for another 1 h. And then the samples were clicked by chemical reaction, separated in SDS-PAGE gel, and visualized as described above.

For target identification by LC-MS/MS, MOVAs were treated with the CGA-p (50 μmol/L) for 4 h in the presence or absence of a competitor (CGA, 4×). The proteins were extracted according to the aforementioned method and conjugated with biotin-azide by a clicked chemistry reaction. Subsequently, the samples were precipitated using pre-chilled acetone and re-dissolved in 1.2% SDS. Streptavidin beads (50 μL) were added to the samples and incubated for 4h at RT. After that, the beads were successively washed with 1% SDS, 0.1% SDS, and 6M urea in PBS. Next, the samples were reduced and alkylated with dithiothreitol (DTT) and iodoacetamide (IAA). The proteins captured by beads were then digested into peptides using trypsin. The peptides in supernatants were collected by centrifugation and desalted using C18 columns. Then, the peptides were labeled using the TMT10 plex reagent according to the MS/MS quantification instructions. Finally, the samples were analyzed by LC-MS/MS (Orbitrap Fusion Lumos, Thermo Fisher Scientific, USA).

2.11.2 Immunofluorescence (IF)

IF was used to characterize the distribution of CGA-p in senescent MOVAs. MOVAs were treated with DOX (200 nmol/L) for 24 h, then incubated with CGA-p (20 μmol/L) for 4 h. The control group was incubated with DMSO. 4% paraformaldehyde (P1110, Solarbio, China) was used to fixature cells for 30 min. The cells were washed with PBS twice, and then incubated with 0.2% triton-100 for 15 min. The cells were conjugated with Rhodmine-N3 by a clicked chemistry reaction for 2 h. Antifade mounting medium with DAPI (P0131, Beyotime, China) was used to sealing the cells. A laser scanning confocal fluorescence microscope (Leica TCS SP8).

2.11.3 Microscale thermophoresis (MST)

MST was employed to quantitatively assess the interaction between CGA and Mettl3. The binding affinity was measured using a Monolith NT.115 (Nano Temper Technologies, Munich, Germany). Briefly, recombinant Mettl3 proteins were labeled with fluorescence using the Monolith His-Tag Labeling Kit (Nano Temper Technologies, Munich, Germany). CGA was serially diluted and mixed with the protein solution

(50% v/v). The mixtures were loaded into capillaries and analyzed using MST at 40% power. The data were processed using MO Affinity Analysis software v2.3.

2.11.4 Cell thermal shift assay (CETSA)

Senescent MOVAs were collected and lysed in PBS added protease and phosphatase inhibitor (P1045, Beyotime). After centrifugation, the supernatant was incubated with 20 μm CGA or DMSO for 2 h at room temperature, and heated with a gradient of 37℃ to 72℃ for 3 min. Then the sample was centrifuged at 12000 r/min 4℃ for 20 min. Collect the supernatant for western blotting.

2.11.5 Statistical analyses

All experiments were repeated independently at least three times. Statistical analyses were performed using GraphPad Prism 8. The results were expressed as mean ± standard error of mean (SEM). For comparisons between 2 groups, unpaired 2-tailed Student t-test was used to determine statistical difference for normally distributed variables; for comparisons of multiple groups, analysis of variance (ANOVA) with Sidak's multiple comparison test was used to compare group means for normally distributed variables. AD incidence and survival were analyzed using Fisher's exact test and log-rank test. Nonparametric Kruskal-Wallis test with Dunn's multiple comparison test was used for non-normally distributed data. $P < 0.05$ was considered to be statistically significant. *$P < 0.05$, **$P < 0.01$, ***$P < 0.001$.

3. Results

3.1 CGA prophylactically prevents AD in vivo.

BAPN, an irreversible and orally active lysyl oxidase (LOX) inhibitor, destroys the structural integrity of the artery wall by inhibiting the crosslink of collagen and elastin [25]. Administration of BAPN constantly can induce AD in mice. To elucidate the impact of CGA intervention on AD, 3-week-old male C57 mice were assigned to four groups: normal, BAPN, CGA-low dose, and CGA-high dose group. Mice in all groups except the normal group were fed with 4% BAPN. Simultaneously, mice in the CGA-low/high dose group received daily intragastric (i.g.) administrations of high-level (150 mg/kg/d) and low-level (30 mg/kg/d) CGA, as depicted in Figure 1A.

Analysis of the survival curve (Figure 1B) and morbidity (Figure 1C) in the AD model mice demonstrated that CGA intervention significantly enhanced the survival rate while reducing the AD incidence and mortality. Typical aortic characteristics revealed that CGA intervention mitigated aortic lesions (Figure 1D). Moreover, CGA decreased the aortic diameters of AD mice (Figure 1E, 1F). These results suggested that CGA can prophylactically prevent AD.

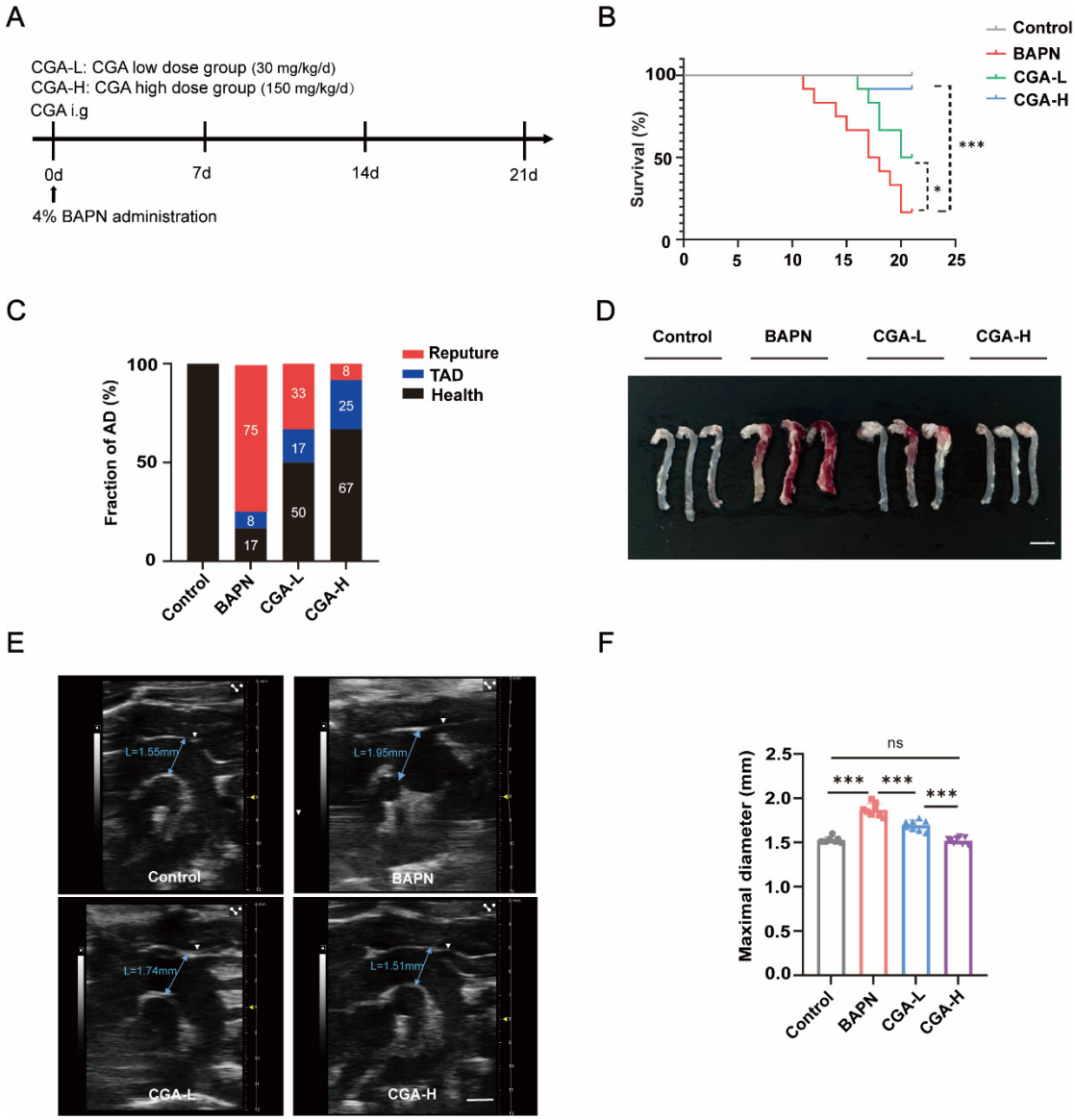

Figure 1 CGA prophylactically prevents AD in vivo. (A) A schematic diagram illustrating the timeline for CGA administration prophylactically in BAPN-induced AD in mice. All mice were 3-week C57 males. Control group, mice treated with normal feed; BAPN group, mice treated with 4% BAPN administration; CGA low dose group, mice treated with 4% BAPN administration and were intragastric administration with CGA 30 mg/kg/d. CGA high dose group, mice treated with 4% BAPN administration and were intragastric administration with CGA 150 mg/kg/d. (B) Survival curve of BAPN treated or untreated mice with low/high dose of CGA treatment as diagram showed. Survival rate was estimated by Kaplan–Meier method and compared by log-rank test (n = 12 mice per group). CGA-L, CGA low dose group; CGA-H, CGA high dose group. *$P < 0.05$, *** $P < 0.001$. (C) The incidence of AD in BAPN treated or untreated mice with low/high dose CGA gavage (n = 12 mice per group). (D) Typical aortic tissue from BAPN treated or untreated mice with low/high dose CGA gavage (n = 3 mice per group). Scale bar, 3.0 mm. (E) Representative ultrasound images showing maximal diameter of ascending aorta. The white triangle is the location of the innominate artery. Scale bar, 1.0 mm. (F) Quantification of maximal diameter for images in (E). Each dot represents maximal diameter of one mouse (n = 8 mice per group). The P-values were calculated by one-way ANOVA with the Sidak's multiple comparison test. Ns, no significance, ***$P < 0.001$. CGA, chlorogenic acid; BAPN, β-aminopropionitrile monofumarate; AD, aortic dissection.

3.2 Evaluation of pathological features of the aorta in dissected mice with CGA intervention.

Pathological staining offers a visual portrayal of the pathological progression of AD. Masson staining takes advantage of the affinity of acidic dyes for collagen fibers, which appear to green-blue [26]. Alcian blue staining is used to detect the abnormal expression of acidic mucopolysaccharides in tissues [27]. Modified Verhoeff Van Gieson elastin staining (EVG) is crucial for studying the structure and integrity of elastic fibers in the aorta [26]. By employing Masson staining (Figure 2A), Alcian Blue staining (Figure 2C), and EVG

staining (Figure 2E), we revealed medial dissection, pseudo lumen formation, and elastic layer disruption. Statistical analysis of the staining results indicated that CGA intervention reduced collagen deposition from 60% to 20% (Figure 2B) and decreased the proteoglycan deposition level from 50% to 20% (Figure 2D). Moreover, it also markedly reduced the incidence of elastic fiber breakage (Figure 2F). These findings suggested that CGA intervention inhibited the pathological progression of AD.

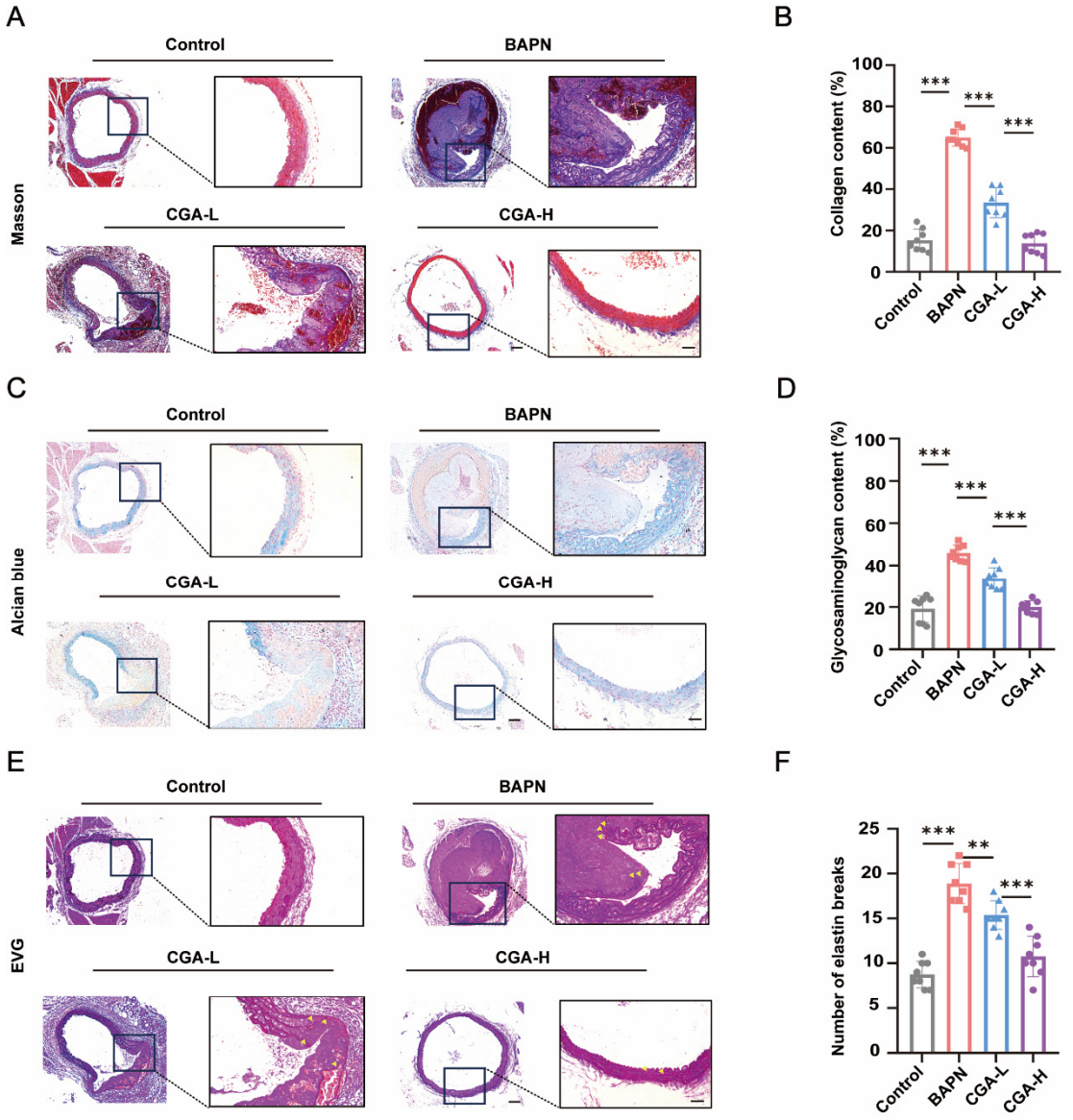

Figure 2 Evaluate pathological features of aorta in dissected mouse with CGA intervention. (A) Representative images showing Masson's trichrome staining in the ascending aorta from the indicated group. Scale bar (left), 200.0 μm; Scale bar (right), 50.0 μm. (B) Bar plots showing the collagen content in ascending aorta (n = 4 mice per group, two sections per mouse). ***$P < 0.001$. (C) Representative images showing Alcian blue staining in the ascending aorta from the indicated group. Scale bar (left), 200.0 μm; Scale bar (right), 50.0 μm. (D) Bar plots showing the proteoglycan content in ascending aorta (n = 4 mice per group, two sections per mouse). ***$P < 0.001$. (E) Representative images showing modified Verhoeff Van Gieson elastin staining (EVG) in the ascending aorta from the indicated group. The arrow indicates elastin breaks. Scale bar (left), 200.0 μm; Scale bar (right), 50.0 μm. (F) Bar plots showing the number of elastin breaks in ascending aorta (n = 4 mice per group, two sections per mouse). The P-values of (B, D, F) were calculated by one-way ANOVA with the Sidak's multiple comparison test. Control group, mice treated with normal feed; BAPN group, mice treated with 4% BAPN administration; CGA low dose group, mice treated with4% BAPN administration and were intragastric administration with CGA 30 mg/kg/d. CGA high dose group, mice treated with 4% BAPN administration and were intragastric administration with CGA 150 mg/kg/d. **$P < 0.01$, ***$P < 0.001$. CGA, chlorogenic acid; BAPN, β-aminopropionitrile monofumarate; AD, aortic dissection; EVG, modified Verhoeff Van Gieson elastin staining.

3.3 Prophylactic CGA inhibits aortic senescence and phenotypic switch in dissected mice.

Given the significant effect of CGA on AD, we further explored how CGA influences AD. By comparing the aorta transcriptome between the CGA intervention and the BAPN group, pathways related to cell senescence and phenotypic switch, such as TNFα-signaling, cytokine-cytokine receptor interactions, and nuclear factor kappa B (*NF-κB)* signaling, were downregulated after CGA intervention (Figure 3A). Meanwhile, differentially expressed genes were subjected to enrichment analysis using the KEGG pathway and gene ontology (GO) classification. A volcano map showed the typical genes involved in these pathways (Figure 3B). The relative expression levels of senescent (*p16, Il-1α, Tnf-α*) (Figure 3C), contractile (*Acta2, Myl9, Tagln*) (Figure 3D) and synthetic (*Col2a1, Mmp25, Cxcl2*) (Figure 3E) gene markers, as revealed by a heat map, were detected by qPCR. The results supported that CGA intervention inhibited the mRNA expression of prominent genes related to senescence and synthesis, restraining phenotypic switch from contractile to synthetic in AD.

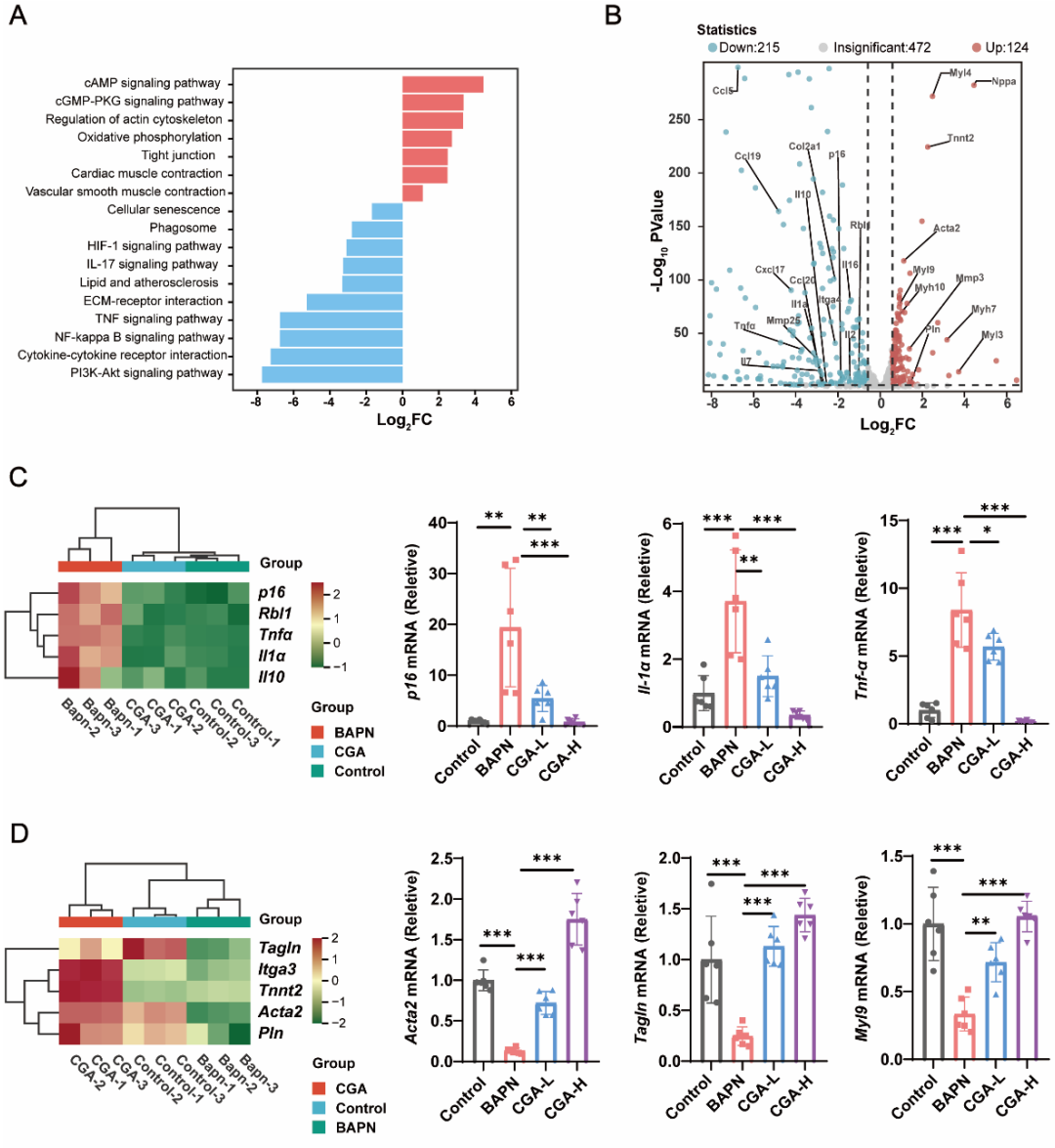

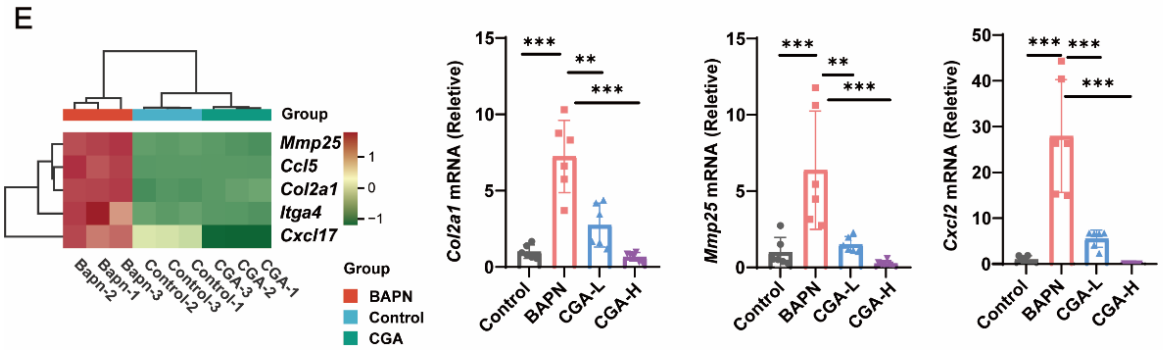

Figure 3 Prophylactic CGA inhibits aortic senescence and phenotypic switch. (A) KEGG enrichment of different signaling pathway of aortic tissues between BAPN-induced mice with or without low-dose CGA treatment. (B) Volcano plot depicting differentially expressed genes in CGA vs BAPN groups. (C) Heatmap showing the comparison of remarkably senescence genes expression on BAPN-induced mice with or without CGA treatment vs control group without any intervention. Transcriptional levels of typical senescence genes (*p16, Il-1α, Tnf-α*) in mice aorta tissues (n = 6 aortic tissues per group) from the indicated group were detected by qPCR. The p-value was calculated by one-way ANOVA with Sidak's multiple comparison test. $*P < 0.05$, $**P < 0.01$, $***P < 0.001$. (D, E) Heatmap showing the comparison of remarkably contractile and synthesis genes expression on BAPN-induced mice with or without CGA treatment vs control group without any intervention. Transcriptional levels of typical contractile genes (*Acta2, Tagln, Myl9*) and synthesis genes (*Col2a1, Mmp25, Cxcl2*) in mice aorta tissues (n = 6 aortic tissues per group) from the indicated group were detected by qPCR. The p-value was calculated as above. $*P < 0.05$, $**P < 0.01$, $***P < 0.001$. KEGG, kyoto encyclopedia of genes and genomes; CGA, chlorogenic acid; BAPN, β-aminopropionitrile monofumarate; AD, aortic dissection; *p16*, cyclin dependent kinase inhibitor 2A; *Il-1α*, interleukin 1 alpha; *Tnf-α*, tumor necrosis factor; *Acta2*, actin alpha 2; *Tagln*, transgelin; *Myl9*, myosin light chain 9; *Col2a1*, collagen type II alpha 1 chain; *Mmp25*, matrix metallopeptidase 25; *Cxcl2*, C-X-C motif chemokine ligand 2.

3.4 CGA interferes with the aging and phenotypic switch of DOX-treated SMCs in vitro.

The DOX-induced cellular senescence model is widely used in aging-related research [28]. The DOX-induced senescence model exhibits typical features of cellular senescence, such as an enlarged and flattened cell morphology, increased SA-β-gal activity, and up-regulation of *p16* and *p21*. Based on the aforementioned findings, we established a DOX-induced model in MOVA to explore the role of CGA on SMC senescence and phenotypic switch. The results of qPCR demonstrated that CGA treatment downregulated the expression of senescent genes (*p53, Il-1β, Rbl1*) (Figure 4A-C), and SA-β-gal staining visually validated the anti-senescent effect of CGA (Figure 4D,4E). Moreover, the increased expression of contractile genes (*Acta2, Ramp1, Myl9*) (Figure 4F-H) and the decreased level of synthesis genes (*Mmp25, Col2a1, Fbn1*) (Figure 4I-K) indicated that CGA suppressed the SMC phenotypic switch. Our findings suggested that CGA has the potential to regulate the induction of contractile gene expression and the inhibition of senescent and synthesis gene expression in DOX-treated MOVAs.

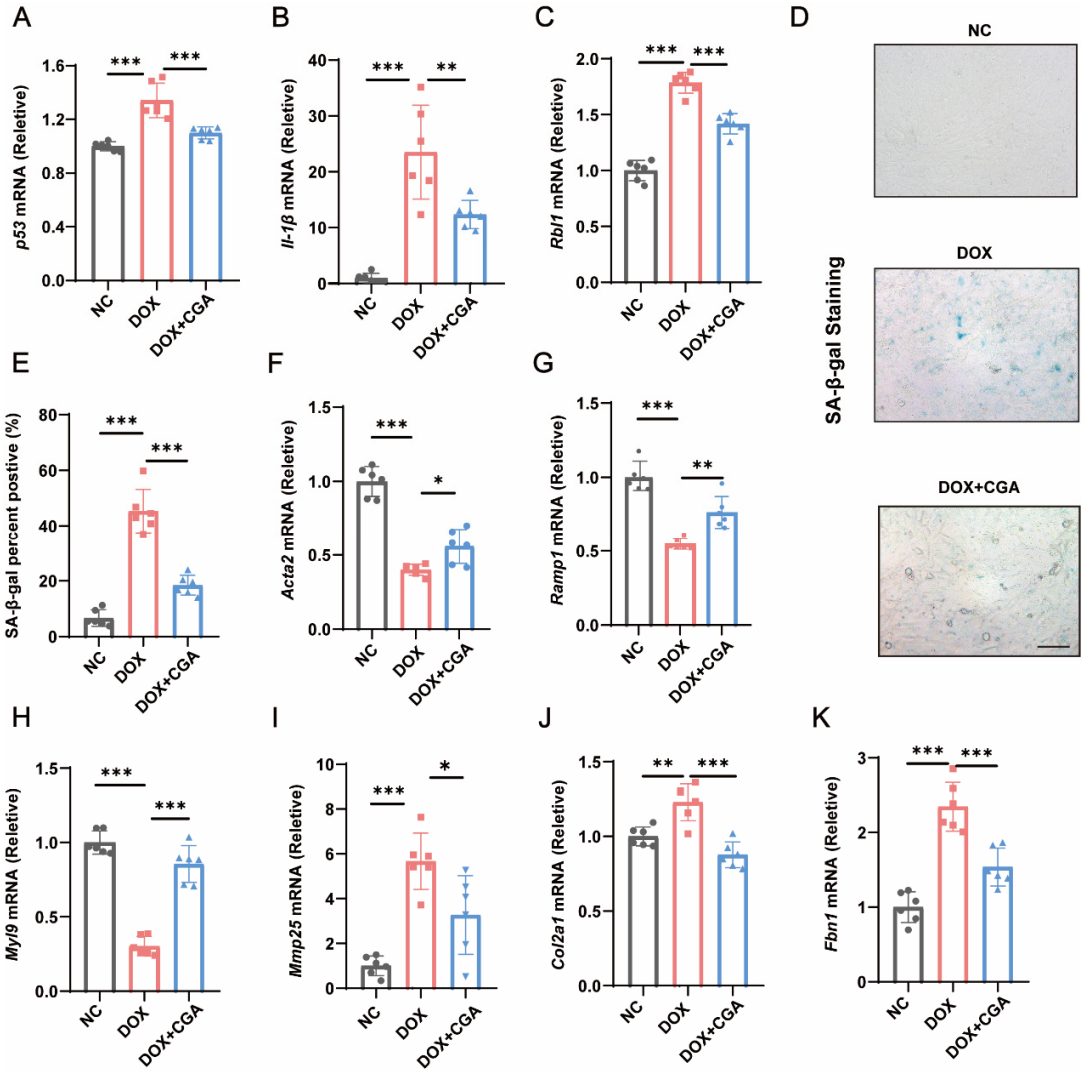

Figure 4 CGA interferes with the aging and phenotypic switch of DOX-treated SMCs in vitro. (A-C) Transcriptional levels of typical senescence genes (*p53, Il-1β, Rbl1*) in DOX (200 nmol/L) -induced MOVAs for 48 h with or without CGA (20 μmol/L) treatment group (n = 6) were detected by qPCR. NC, negative control; DOX, the group treated with DOX 200 nmol/L for 48 h; DOX+CGA, the group treated with DOX 200 nmol/L and CGA 20 μmol/L for 48 h. The p-value was calculated by one-way ANOVA with Sidak's multiple comparison test. $^{**}P < 0.01$, $^{***}P < 0.001$. (D, E) Representative images of SA-β-gal staining (D) and quantification (E) in the indicated groups. (n = 6). Statistical analysis was performed by one-way ANOVA followed by Tukey's multiple comparison test. Scale bar, 100 μm. $^{***}P < 0.001$. (F-K) Transcriptional levels of typical contractile (*Acta2, Ramp1, Myl9*) and synthesis genes (*Mmp25, Col2a1, Fbn1*) in DOX (200 nmol/L) -induced MOVAs with or without CGA (20 μmol/L) treatment group (n = 6) were detected by qPCR. The p-value was calculated as above. $^{*}P < 0.05$, $^{**}P < 0.01$, $^{***}P < 0.001$. DOX, doxorubicin; CGA, chlorogenic acid; MOVA, mouse aortic vascular smooth cell; SA-β-gal, senescence-associated-β-galactosidase; *p53*, tumor protein p53; *Il-1β*, interleukin 1 beta; *Rbl1*, RB transcriptional corepressor like 1; *Acta2*, Actin Alpha 2; *Tagln*, transgelin; *Ramp1*, receptor activity modifying protein 1; *Myl9*, myosin light chain 9; *Col2a1*, collagen type II alpha 1 chain; *Mmp25*, matrix metallopeptidase 25; *Fbn1*, fibrillin 1.

3.5 CGA therapeutically arrests AD in vivo.

Prophylactic administration primarily simulates the effects of CGA intervention in the early and middle stages of AD. Due to lacking valid screening indicators, therapeutic administration is closer to the clinical experiment. We further sought to identify the therapeutical effect of CGA in arresting AD. We used 4% BAPN-fed mice to establish the AD model. Once the first mouse died for AD, we initiated the administration of CGA (Figure 5A). Consistent with the prophylactical CGA-intervention, CGA therapeutically reduced dissection mortality (Figure 5B) and morbidity (Figure 5C). Evidently, the typical mouse aortas verified the

therapeutic function of CGA (Figure 5D). By measuring the aortic diameter using imageJ, the results showed that CGA intervention reduced aortic dilation in AD model (Figure 5E). Furthermore, mouse aorta sections were stained for pathological features. The results of Masson, Alcian blue and EVG staining indicated that CGA inhibited collagen deposition, proteoglycan deposition, and elastic fiber breakage (Figure 5F-H). Together, the therapeutic CGA intervention can halt the progression of AD.

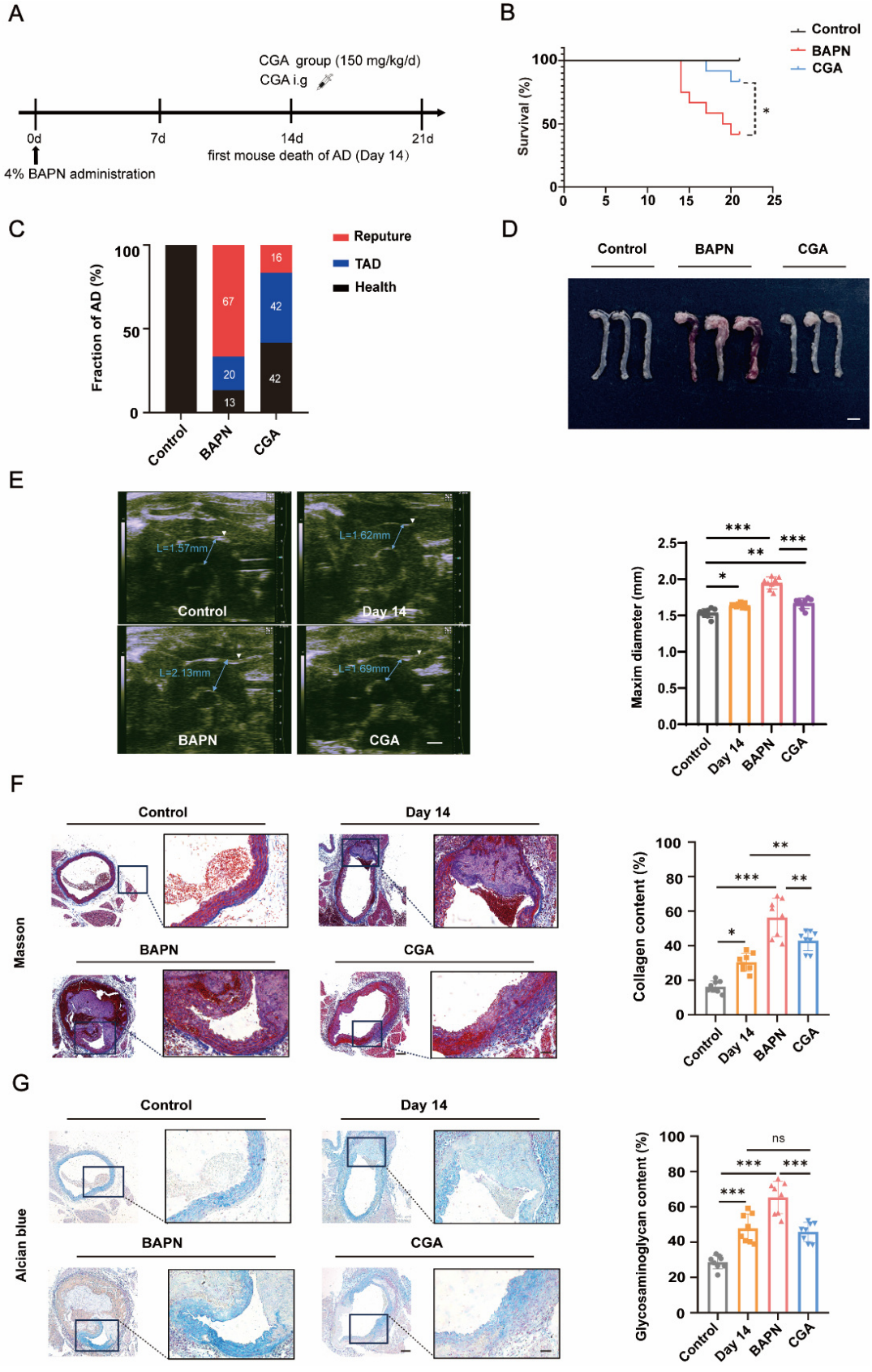

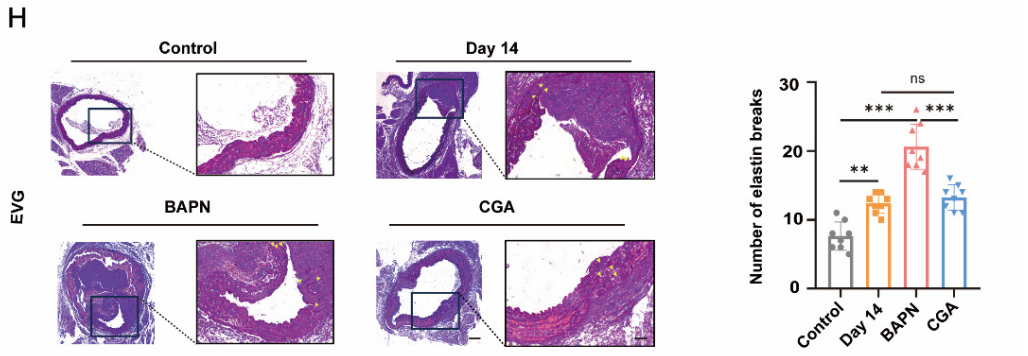

Figure 5 CGA therapeutically arrests AD in vivo. (A) A schematic diagram illustrating the timeline for CGA administration therapeutically in BAPN-induced AD in mice. All mice were 3-week C57 males. Control group, mice treated with normal feed; BAPN group, mice treated with 4% BAPN administration; CGA group, mice treated with 4% BAPN administration from Day0, then were intragastric administration with CGA 150 mg/kg/d when the first mouse death for AD (Day 14). (B) Survival curve of BAPN treated or untreated mice with CGA treatment as diagram showed. Survival rate was estimated by Kaplan–Meier method and compared by log-rank test (n = 12 mice per group). *$P < 0.05$. (C) The incidence of AD in BAPN-induced mice with CGA treatment as the indicated group (n = 12 mice per group). (D) Typical aortic tissue from the indicated group (n = 3 mice per group). Scale bar, 3.0 mm. (E) Representative ultrasound images (left) and quantification of maximal diameter for images (right) showing maximal diameter of ascending aorta. The white triangle is the location of the innominate artery. Day 14 group, the mice induced with 4% BAPN until the first mouse died for AD, the mice were detected by ultrasound and sacrificed. Scale bar (left), 1.0 mm. Each dot represents maximal diameter of one mouse (right) (n = 8 mice per group). *$P < 0.05$, **$P < 0.01$, ***$P < 0.001$. (F-H) Representative images showing Masson's trichrome (F), Alcian blue (G) and EVG (H) staining in the ascending aorta from the indicated group. The arrow indicates elastin breaks. Bar plots showing the collagen content (F), proteoglycan content (G) and the number of elastin breaks (H) in ascending aorta (n = 4 mice per group, two sections per mouse). Scale bar (left), 200.0 μm; Scale bar (right), 50.0 μm. *$P < 0.05$, **$P < 0.01$, ***$P < 0.001$. The P-values were calculated by one-way ANOVA with the Sidak's multiple comparison test. CGA, chlorogenic acid; BAPN, β-aminopropionitrile monofumarate; AD, aortic dissection; EVG, modified Verhoeff Van Gieson elastin staining.

3.6 CGA therapeutically reduces aortic senescence and phenotypic switch in dissected mice.

We next investigated how CGA regulates aortic senescence and phenotypic switch to arrest AD. Based on the above-mentioned transcriptome results, we selected typical senescent, contractile and synthetic genes for qPCR. The data of the aortic tissues revealed that CGA intervention decreased the expression of senescent (*p16, Il-1α, Tnf-α*) (Figure 6A-C) and synthetic genes (*Col2a1, Mmp25, Cxcl2*) (Figure 6G-I), while the expression of contractile gene increased (*Acta2, Tagln, Myl9)* (Figure 6D-G). Comparing the gene expression at the end of the AD with those at the beginning (Day 14 group *vs* CGA group), the results suggested that therapeutical CGA intervention could not reverse progress of AD but could arrest it. When MOVAs were treated with DOX, CGA suppressed the expression of senescent genes (*p21, p16, Tnf-α*) (Figure 6J-K), and SA-β-gal staining activity was also significantly inhibited (Figure 6M, 6N). The contractile genes were strongly positive associating with CGA intervention in MOVAs (*Acta2, Myl9, Ramp1*) (Figure 6O-Q), in contrast the synthetic genes were negative associating with CGA (*Col2a1, Cxcl2, Fbn1*) (Figure 6R-T). These data confirmed that CGA modulated AD both *in vivo* and *in vitro* by regulating aortic senescence and phenotypic switch.

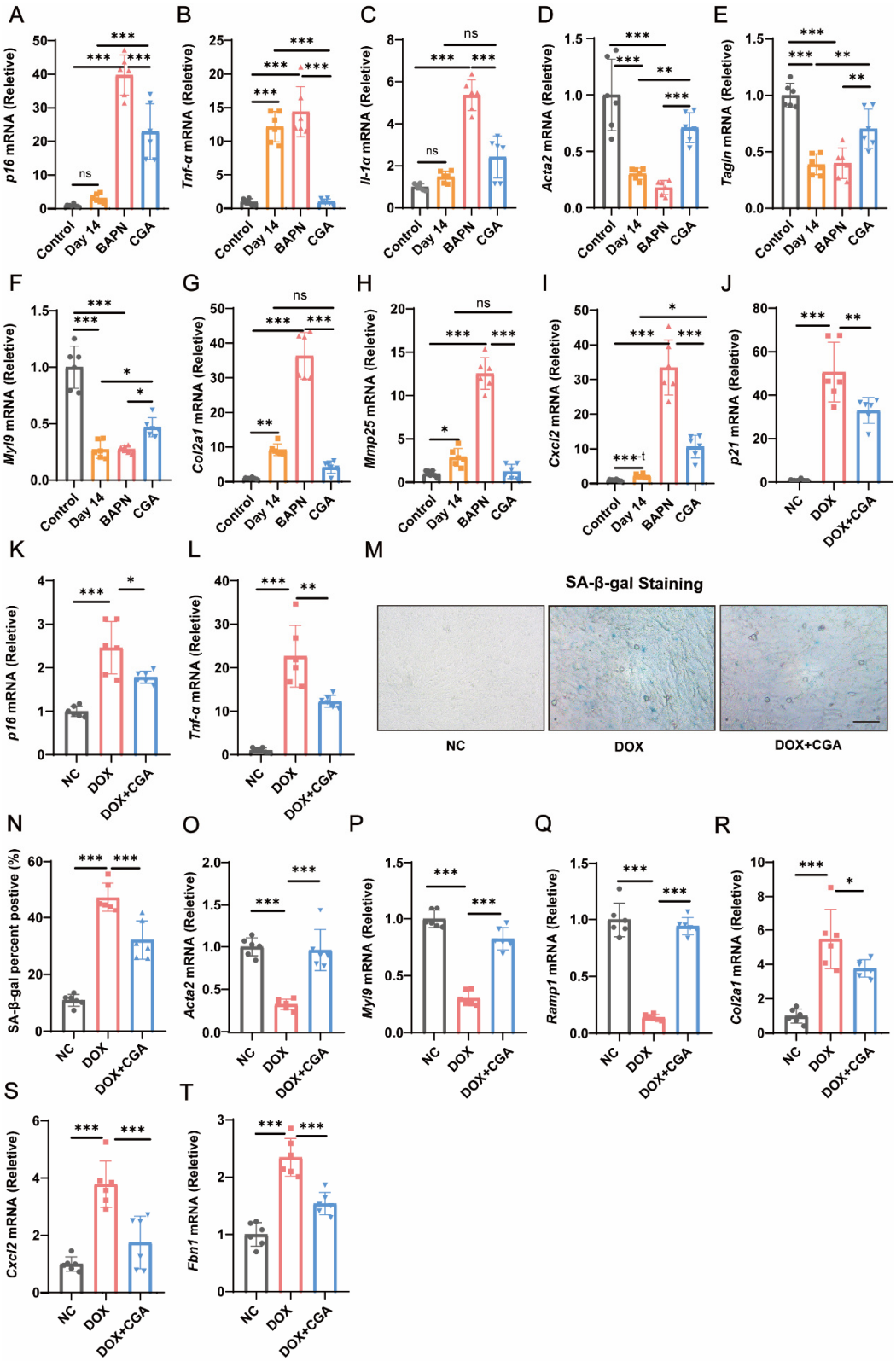

Figure 6 CGA therapeutically reduces aortic senescence and phenotypic switch. (A-I) Transcriptional levels of typical senescence (*p16, Tnf-α, Il-1α*) (A-C), contractile (*Acta2, Tagln, Myl9*) (D-F) and synthesis (*Col2a1, Mmp25, Cxcl2*) (G - I) genes in mice aorta tissues (n = 6 aortic tissues per group) were detected by qPCR. The p-value was calculated by one-way ANOVA with Sidak's multiple comparison test. Control group, mice treated with normal feed; BAPN group, mice treated with 4% BAPN administration; CGA group, mice treated with 4% BAPN administration from Day0, then were intragastric administration with CGA 150 mg/kg when the first mouse death for AD (Day 14). ns, no significance, $*P < 0.05$, $**P < 0.01$, $***P < 0.001$. (J-L) Transcriptional levels of typical senescence genes (*p21*, *p16, Tnf-α*) in MOVAs, which was induced by DOX (200 nmol/L) for 24 h, then treated with or without CGA (20 μmol/L) for 24 h, were detected by qPCR (n = 6). NC, negative control; DOX, the group treated with DOX 200 nmol/L for 48 h; DOX+CGA, the group treated with DOX 200 nmol/L for 24 h, and stimulated with CGA 20 μmol/L for another 24 h. The p-value was calculated as above. $*P < 0.05$, $**P$

< 0.01, ***P < 0.001. (M, N) Representative images of SA-β-gal staining (M) and quantification (N) in the indicated groups. (n = 6). Statistical analysis was performed as above. Scale bar, 100 μm. ***P < 0.001. (O-T) Transcriptional levels of typical contractile (*Acta2, Myl9, Ramp1*) and synthesis genes (*Col2a1, Cxcl2, Fbn1*) in MOVAs, which was performed to CGA for 24 h after being induced by DOX (200 nmol/L) for 24 h, were detected by qPCR (n = 6). The p-value was calculated by one-way ANOVA with Sidak's multiple comparison test. *P < 0.05, ***P < 0.001. CGA, chlorogenic acid; DOX, doxorubicin; MOVA, mouse aortic vascular smooth cell; SA-β-gal, senescence-associated-β-galactosidase; one-way ANOVA, one-way analysis of variance. *p16*, cyclin dependent kinase inhibitor 2A; *Il-1α*, interleukin 1 alpha; *Tnf-α*, tumor necrosis factor; *Acta2*, Actin Alpha 2; *Tagln*, transgelin; *Myl9*, myosin light chain 9; *Col2a1*, collagen type II alpha 1 chain; *Mmp25*, matrix metallopeptidase 25; *Cxcl2*, C-X-C motif chemokine ligand 2; *p21*, cyclin dependent kinase inhibitor 1A; *Ramp1*, receptor activity modifying protein 1; *Fbn1*, fibrillin 1.

3.7 The ABPP technique identifies that CGA may target Mettl3 to alleviate dissection.

To comprehensively profile the direct target of CGA in senescent SMCs, ABPP was employed to identify the potential proteins covalently binding to CGA (Figure 7A). In this strategy, a chemical probe with an alkyne handle tag was designed and synthesized, and then incubated with living cells. The proteins binding to the probe could be fluorescently visualized after conjugating with a fluorescent dye via a copper-catalyzed azide–alkyne cycloaddition (CuAAC) reaction. Additionally, the protein targets could be further enriched through biotin-avidin interaction and further identified by LC-MS/MS. Compared with CGA, an analog with a hydrogenated double bond nearly loses its biological activity in regulating senescent SMCs (Figure 7B and 7C), suggesting the crucial role of its unsaturated ketone structure in binding to protein targets. Next, a CGA chemical probe (CGA-p) that we previously reported was used to perform ABPP (Figure 7B). Senescent MOVAs treated with CGA-p exhibited the reduced expression of senescent (*p16, p53*) and contractile (*Col2a1, Ccl5*) markers (Figure S4). Adding the fluorescent group Rhodamine-N3 to the CGA-p through the click reaction, the distribution of the probe in senescent MOVAs were observed by a fluorescence confocal microscope. We found that the CGA-p signal (red) was mainly distributed in the cytoplasm (Figure S5). As shown in Fig. 7D, the label intensity of the CGA probe on the proteins was dose dependent, implying that the proteins were successfully captured by the probe. Moreover, an excess of CGA could compete away the labeling effect of the CGA probe on proteins in a dose-dependent manner (Figure 7E), suggesting that CGA and its probe shared the protein targets and that the chemical modification on CGA did not hamper the ability of binding proteins. After a cutoff of fold change > 2.0 and p-value < 0.05 was applied, the volcano plots showed that 220 targets were identified (Figure 7F). By comparing protein abundance between the competition group and the CGA-p group, we identified Mettl3 as the potential factor driving SMCs senescence and phenotypic switch. Additionally, the dissociation constant (Kd) between Mettl3 and CGA was measured as 7.96 μM using MST (Figure 7G). Further, the interaction between Mettl3 and CGA was confirmed by CETSA (Figure 7H, I), as indicated that Mettl3 had the higher thermal stability after CGA treatment. Collectively, Mettl3 was identified as a potential target of CGA in senescent SMCs. These findings suggest that CGA may target Mettl3 to alleviate AD.

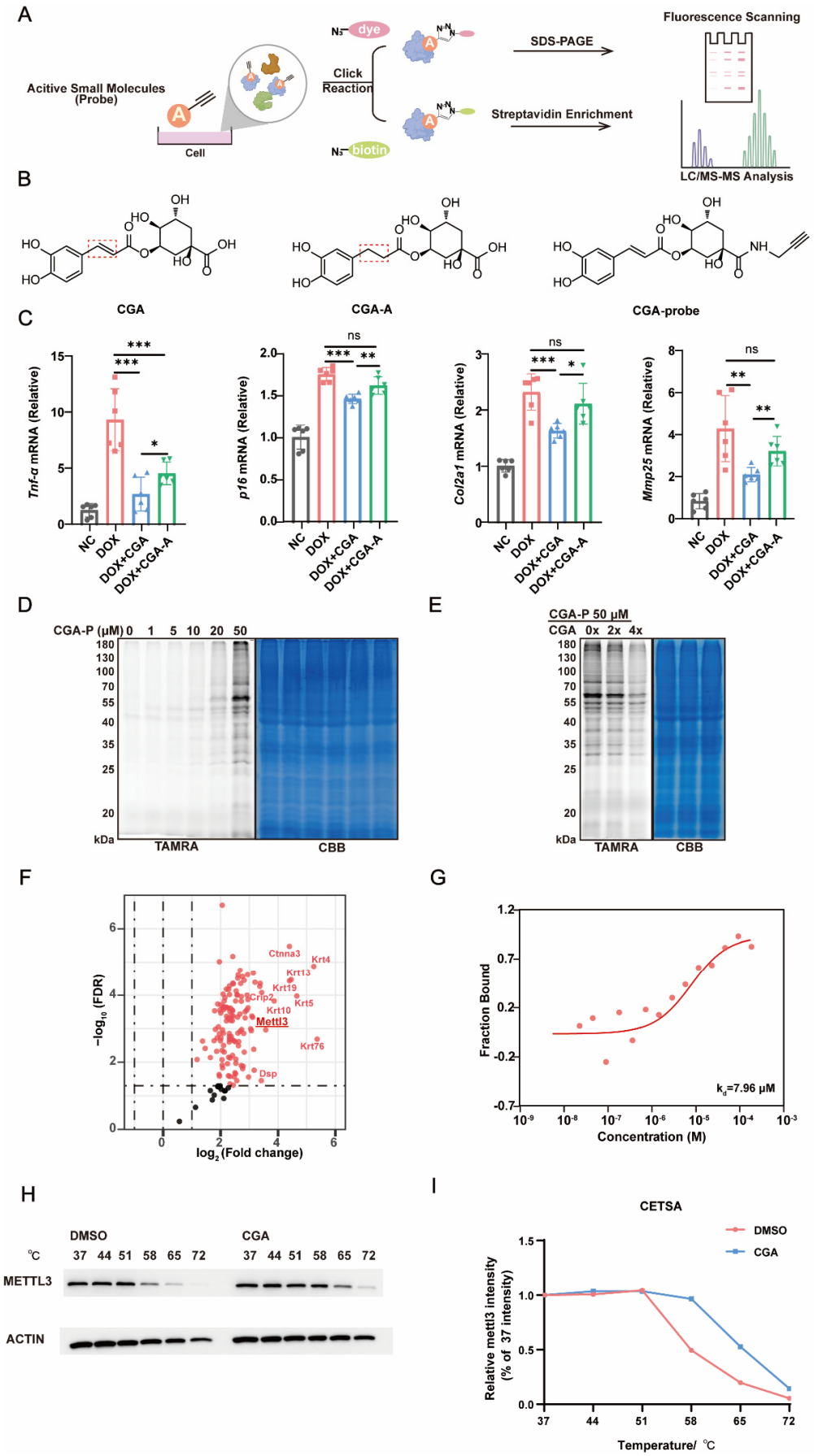

Figure 7 The ABPP technique identified that CGA may targets Mettl3 to relieve dissection. (A) Workflow of the strategy combining ABPP and click chemistry (schematic). (B) Chlorogenic acid (CGA), chlorogenic acid analogue (CGA-A) and chlorogenic acid probe (CGA-p) chemical structure. (C) Transcriptional levels of typical senescence (*Tnf-α, p16*) and synthesis (*Col2a1, Mmp25*) genes in DOX (200 nmol/L) -induced MOVAs for 48 h with CGA (20 μmol/L) or CGA-A (20 μmol/L) treatment group (n = 6) were detected by qPCR. NC, negative control; DOX, the group treated with DOX 200 nmol/L

for 48 h; DOX+CGA, the group treated with DOX 200 nmol/L and CGA 20 μmol/L for 48 h; DOX+CGA-A, the group treated with DOX 200 nmol/L and CGA-A 20 μmol/L for 48 h. The p-value was calculated by one-way analysis of variance (ANOVA) with Sidak's multiple comparison test. ns, no significance, *$P < 0.05$, **$P < 0.01$, ***$P < 0.001$. (D) The labeling of situ protein labeling with CGA-p in MOVAs treating with DOX (200 nm). (E) Excess CGA competed with labeled protein for binding to CGA-p in situ. (F) Volcano plot of the pulldown and identified proteins (bold red points) in CGA vs. DMSO groups by ABPP. (G) Microscale Thermophoresis showing the binding kinetics between CGA and Mettl3. (H) The interactions between CGA and Mettl3 confirmed by CETSA-WB. (I) Quantitative statistics of CETSA-WB experiment. CGA, chlorogenic acid; CGA-A, chlorogenic acid analogue; *Tnf-α*, tumor necrosis factor; *p16*, cyclin dependent kinase inhibitor 2A; *Col2a1*, collagen type II alpha 1 chain; *Mmp25*, matrix metallopeptidase 25; DOX, doxorubicin; MOVA, mouse aortic vascular smooth cell; CGA-p, chlorogenic acid probe; one-way ANOVA, one-way analysis of variance. CETSA, cell thermal shift assay. WB, western blotting.

3.8 Mettl3 regulates the senescence and phenotypic switch in vitro.

To validate the modulation of Mettl3 on SMC senescence and phenotypic switch, we utilized Mettl3 inhibitor STM2457 to treat MOVAs *in vitro*. Consistent with CGA intervention, STM2457 treatment in the DOX-induced senescent cells alleviated SMCs senescence and phenotypic switch. The results of qPCR revealed that, compared to the DOX-induced group, STM2457 reduced the expression of senescent genes (*p16, Il-1α, Rbl1, Tagln*) (Figure 8A-C). Moreover, the increased expression of contractile genes (*Acta2, Ramp1, Myl9*) (Figure 8D-F) and the decreased levels of synthetic genes (*Col2a1, Cxcl2, Mmp25*) (Figure 8G-I) indicated that STM2457 suppressed SMCs phenotypic switch. In contrast, the overexpression of Mettl3 made the intervention of CGA in senescent MOVAs ineffective (Figure 8J, K), suggesting that Mettl3 is the key of CGA to arrest AD. Recent studies have revealed that AP-1 played important roles in AD [12]. Moreover, Mettl3 has been reported to regulate the expression of JUN (AP-1 transcription factor subunit) [23]. Subsequently, we examined the effect of CGA as well as STM2457 on the expression of JUN in senescent MOVAs. The results indicated that both of the treatments significantly reduced the protein level of JUN in senescent MOVAs (Figure 8L). We also found the inhibitory effects of CGA and STM2457 on the expression of SMCs senescent (*p16*) and phenotypic switch (*Acta2, Col2a1*) markers (Figure 8M). Collectively, these results suggested that CGA-mediated SMCs senescent and phenotypic switch regulation was associated with Mettl3 and JUN signaling in *vitro*.

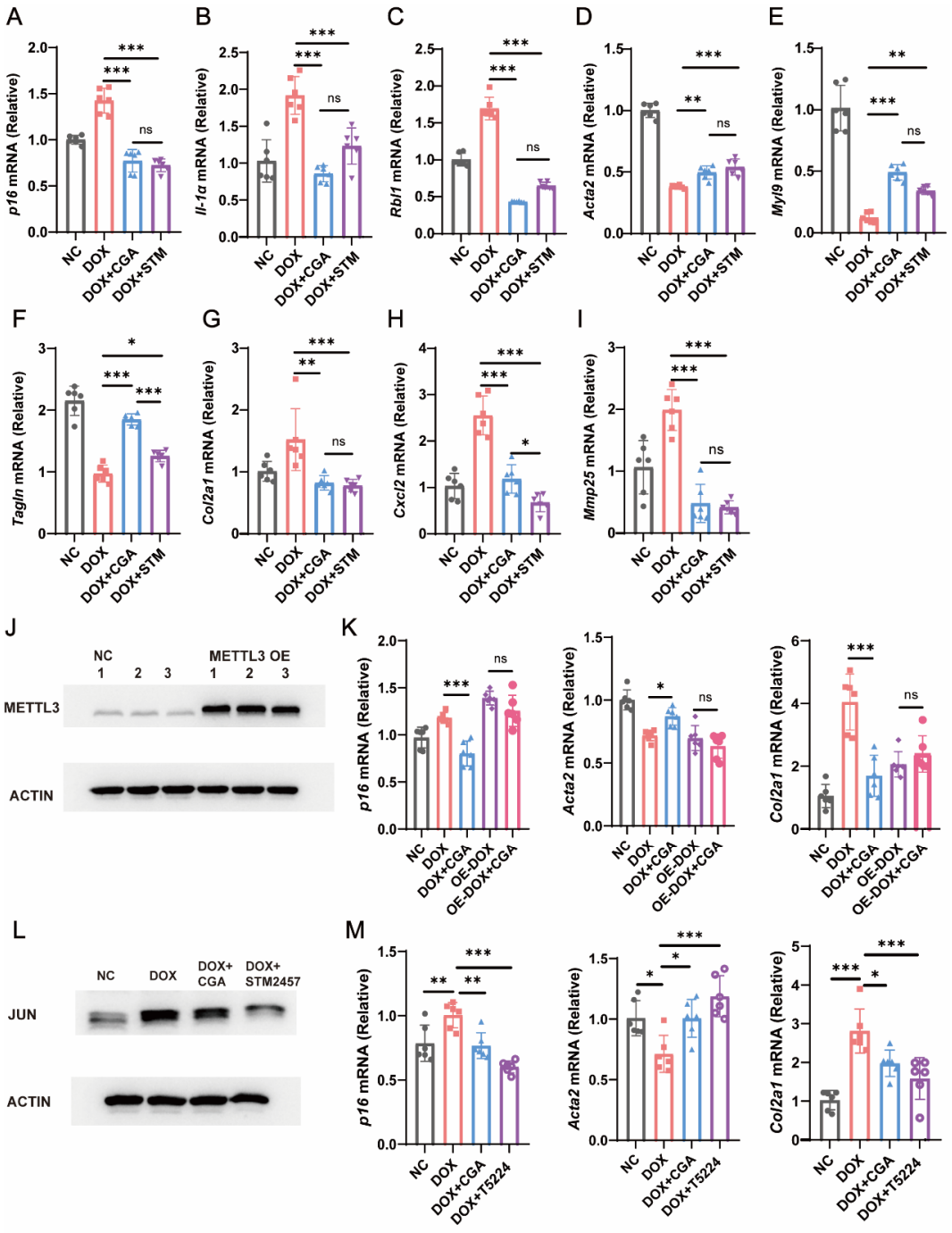

Figure 8 Mettl3 inhibitor reduces the senescence and phenotypic switch in DOX-induced model. (A-I) Transcriptional levels of typical senescence (*p16, Il-1α, Rbl1*), contractile (*Acta2, Myl9, Tagln*) and synthesis (*Col2a1, Cxcl2, Mmp25*) genes from the indicated group (n = 6) were detected by qPCR. STM-STM2457, the inhibitor of Mettl3. NC, negative control; DOX, the group treated with DOX 200 nmol/L for 48 h; DOX+CGA, the group treated with DOX 200 nmol/L and CGA 20 μmol/L for 48 h; DOX+STM, the group treated with DOX 200 nmol/L and STM 5 μmol/L for 48 h. The p-value was calculated by one-way ANOVA with Sidak's multiple comparison test. ns, no significance, $*P < 0.05$, $**P < 0.01$, $***P < 0.001$. (J) Detection of the transfection effect of METTL3 overexpression (OE) plasmid to MOVA by western blotting. n = 3. (K) Transcriptional levels of typical senescence genes (*p16*), contractile (*Acta2*) and synthesis genes (*Col2a1)* in MOVAs and METTL3 OE MOVAs, which was induced by DOX (200 nmol/L) for 24 h, then treated with or without CGA (20 μmol/L) for 24 h, were detected by qPCR (n = 6). NC, negative control; DOX, the group treated with DOX 200 nmol/L for 48 h; DOX+CGA, the group treated with DOX 200 nmol/L for 24 h, and stimulated with CGA 20 μmol/L for another 24 h. OE-DOX/OE-DOX+CGA, the cells were pre-transfected with the METTL3 OE plasmid. The p-value was calculated by one-way ANOVA with Sidak's multiple comparison test. The p-value of t-*** was calculated by t-test. $*P < 0.05$, $**P < 0.01$, $***P < 0.001$. ns, no significance. (L) Detect the expression of AP-1 (JUN) in senescent MOVAs stimulated with STM2457 by WB. The groups were treated as above. The p-value was calculated by one-way ANOVA with Sidak's multiple

comparison test. ns, no significance, *$P < 0.05$, **$P < 0.01$, ***$P < 0.001$. (M) Transcriptional levels of typical senescence (*p16*), contractile (*Acta2*) and synthesis (*Col2a1*) markers after T5224 stimulates senescent MOVAs (n = 6). T5224, AP-1 inhibitor. NC, negative control; DOX, the group treated with DOX 200 nmol/L for 48 h; DOX+CGA, the group treated with DOX 200 nmol/L and CGA 20 μmol/L for 48 h; DOX+T5224, the group treated with DOX 200 nmol/L and T5224 40μmol/L for 48 h. The p-value was calculated by one-way ANOVA with Sidak's multiple comparison test. ns, no significance, *P < 0.05, **P < 0.01, ***P < 0.001.*p16*, cyclin dependent kinase inhibitor 2A; *Il-1α*, interleukin 1 alpha; *Rbl1*, RB transcriptional corepressor like 1; *Acta2*, Actin Alpha 2; *Myl9*, myosin light chain 9; *Tagln*, transgelin; *Col2a1*, collagen type II alpha 1 chain; *Cxcl2*, C-X-C motif chemokine ligand 2; *Mmp25*, matrix metallopeptidase 25; CGA, chlorogenic acid; AD, aortic dissection; WB, western blotting.

3.9 Mettl3 inhibitor therapeutically arrests aortic dissection in vivo.

Finally, to test Mettl3 as a protein target in AD treatment, we constructed intervention experiment in mice: 3-week-old mice were induced AD by 4% BAPN feed. And when the first mouse died for AD, STM2457 was intraperitoneal injection (30 mg/kg.d daily) to model mice (Figure S6A). The survival curve showed that STM2457 significantly inhibited the death of AD model mice (Figure S6B). Compared with BAPN group, STM2457 i.p. reduced the ratio of reputation in AD (Figure S6C). Aortic diameters results indicated that STM2457 intervention decreased abnormal aortic dilation in the AD (Figure S6E). Moreover, we performed the pathological staining of the aorta for each group, including Masson, Alcian blue and EVG staining. The results demonstrated that STM2457 prevented the collagen deposition, proteoglycan deposition, and elastic fiber breakage of the aorta in mice (Figure S6F-6H). Collectively, our results indicated that inhibition of Mettl3 therapeutically arrests aortic dissection *in vivo*.

4. Discussion

Accumulating evidence has strongly indicated that the senescence and phenotypic switch of SMCs are crucial pathological features of AD [29,30]. Given this, targeting the phenotypic transformation and senescence of SMCs may serve as effective intervention strategies for AD. CGA, a potent anti-inflammatory compound [31], was selected to intervene the process of inflammation-induced phenotypic transformation in AD. In this study, both prophylactical and therapeutical interventions with CGA in a BAPN-induced mouse model effectively alleviated the mortality and morbidity of AD. Subsequent RNA transcriptome sequencing results revealed that CGA intervention downregulated the pathways associated with inflammation and phenotypic switch. Notably, senescence-related pathways were also downregulated. Although the relationship between senescence and phenotypic switch remains uncertain, anti-senescence is undoubtedly a significant approach for CGA to halt the development of AD. Moreover, experiments *in vitro* demonstrated that CGA intervention inhibited SMCs senescence while simultaneously suppressed the phenotypic switch from contractile to synthetic. Subsequently, employing CGA probes, we screened and identified Mettl3 as a high confidence CGA-binding protein by integrating ABPP and MST. The Mettl3 inhibitor-STM2457 was verified to decrease the level of senescence and phenotypic switch markers. Thus, it can be concluded that Mettl3 mediated the inhibitory effect of CGA on SMCs senescence and phenotypic switch, thereby arresting the development of AD.

CGA has a great potential to interfere with AD by its anti-inflammation function. CGA, a polyphenolic compound widely present in plants [32], has attracted increasing attention for its potential effects in

cardiovascular diseases [33]. CGA can downregulate the expression of pro-inflammatory cytokines, such as *Tnf-α*, *Il-6* and*Il-1β* [34]. Additionally, the activation of *NF-κB*, a transcription factor involved in the regulation of the inflammatory response, was inhibited by CGA [35]. In most cardiovascular diseases, inflammation is considered a risk factor. A recent study indicated a tight connection between inflammation and the incidence of AD: *TNF-α*, a powerful pro-inflammatory factor, initiates vascular degeneration in AD by triggering a stress-responsive transcriptional programme leading to SMC phenotypic switch [12]. Our results revealed that CGA as an anti-inflammation compound depressed the progression of AD in the BAPN-induced mouse model. In addition, our results also proved that CGA intervention can prevent phenotypic switch from contractile to synthetic in AD.

CGA not only prevents phenotypic switch but also blocks SMCs senescence, which cooperatively resists the further development of AD. SMCs senescence has been identified to participant in the formation of AD. A previous study showed that the expression of sirtuin 1 is decreased in AD, and the reduction of sirtuin 1 aggravates SMCs senescence and the AD incidence [36]. Another study showed that MYLK overexpression reversed miR-1204-induced VSMCs senescence, SASP, and contractile phenotypic changes, as well as the aggravation of AD [19]. Many factors in SASP are pro-inflammatory cytokines and chemokines, such as IL-6 and TNF-α. The inflammatory microenvironment established by SASP can contribute to the development and progression of senescence in AD. Although the causal relationship between senescence and inflammation is unclear, anti-senescence precisely alleviates inflammation stress and reduces the occurrence of AD. Here, we observed that the senescence-related pathways were down-regulated in the CGA group compared to the BAPN group, and SA-β-gal staining showed less accumulation of aging markers. In a study on the impact of CGA on skin cells, it was demonstrated that CGA could inhibit skin cell senescence by reducing the level of inflammation [22,37]. These findings suggested that CGA may arrest the development of AD by inhibiting SMCs senescence and phenotypic switch.

Furthermore, we verified Mettl3 as a downstream factor of CGA by utilizing ABPP. On the one hand, Mettl3 plays a role in regulating cell differentiation. By adding N6-methyladenosine (m6A) modifications to specific mRNAs, Mettl3 can influence the translation efficiency and stability of genes related to cell differentiation [38]. Phenotypic transformation can be regarded as a specific type of cell differentiation in which cells lose their terminal differentiation state. On the other hand, a recent study has shown that Mettl3-mediated m6A modification of genes related to the cell-cycle regulatory machinery, such as *p21* and *p16*, is involved in the senescence-associated signaling pathways [40]. By using the Mettl3 inhibitor to treat senescent SMCs, we observed that the expression levels of senescence and synthetic SMCs markers were reduced. Current research suggested that AP-1 is the main factor involved in AD [12], and also regulated by m6A methylation [23]. We examined the expression of JUN in senescent MOVAs intervened by STM2457 and CGA, and found that AP-1 was involved in Mettl3-mediated regulation of SMC senescence and phenotypic switch. Mettl3 inhibitor was also used to treat with AD model mice, and a series of evidence indicated the efficacy of STM2457 to AD *in vivo*. Senescence and phenotypic switch markers of the mouse

aorta were detected (Figure S7). Therefore, CGA may inhibit senescence and phenotypic switch by binding to Mettl3 to suppress the progression of AD.

In our study, CGA exhibited a remarkable prophylactic effect in AD. As a compound widely distributed in plants, CGA is abundant in coffee beans, as well as fruits and vegetables [40]. Under normal dietary conditions, the intake of CGA from natural food sources is generally considered safe. Long-term daily consumption of CGA within the normal range of dietary exposure does not pose a risk to human health [41]. For example, studies on the consumption of coffee, which is a rich source of CGA, have not found significant adverse effects on the health of the general population when consumed in moderation [42]. Therefore, increasing the dietary intake of CGA may be an effective management to lower the risk of AD [44].

5. Conclusion

Through both prophylactic and therapeutic interventions with CGA, we have identified that CGA can effectively suppress the development of AD. Integrating transcriptome sequencing data with *in vitro* and *in vivo* model interventions, we further determined that CGA inhibits AD by reducing the phenotypic switch and senescence of SMCs. Furthermore, a CGA probe was constructed to explore targets via ABPP, and Mettl3 was identified as an important target of CGA in senescent SMCs. Mettl3 regulates the phenotypic switch and senescence of SMCs, thereby arresting the progression of AD. Our findings offer novel insights into the management of AD, highlighting the CGA-mediated interventions as a promising strategy for AD prevention and treatment.

Abbreviations: AD, aortic dissection; CGA, chlorogenic acid; BAPN, β-aminopropionitrile; DOX, doxorubicin; VSMCs, vascular smooth muscle cells; qPCR, quantitative polymerase chain reaction; p16, cyclin dependent kinase inhibitor 2A; Il-1α, interleukin 1 alpha; Tnf-α, tumor necrosis factor; Acta2, actin alpha 2; Tagln, transgelin; Myl9, myosin light chain 9; Col2a1, collagen type II alpha 1 chain; Mmp25, matrix metallopeptidase 25; Cxcl2, C-X-C motif chemokine ligand 2; MOVA, mouse aortic vascular smooth cell; SA-β-gal, senescence-associated β-galactosidase; WB, western blotting; ABPP, activity-based protein profiling; CuAAC, copper-catalyzed azide–alkyne cycloaddition; LC-MS/MS, liquid chromatography-tandem mass spectrometry; MST, microscale thermophoresis; CETSA, cell thermal shift assay; SASP, senescence-associated secretory phenotype.

Funding: This work was supported by the Beijing Advanced Innovation Center for Food Nutrition and Human Health, the National Natural Science Foundation of China (82470442, 82170429), the State Key Laboratory of Cardiovascular Disease, Fuwai Hospital, Chinese Academy of Medical Sciences (2024GZkf-05).

Conflicts of Interest

The authors declare no conflict of interest.

Reference

1. Isselbacher EM, Preventza O, Hamilton Black J, Augoustides JG, Beck AW, Bolen MA, et al. 2022 ACC/AHA Guideline for the Diagnosis and Management of Aortic Disease: A Report of the American Heart Association/American College of Cardiology Joint Committee on Clinical Practice Guidelines. Circulation. 2022;146:e334–482.
2. Hofmann Bowman MA, Eagle KA. Gene-Based Management for Thoracic Aortic Disease. J Am Coll Cardiol. 2022;80:870–2.
3. Elefteriades JA, Farkas EA. Thoracic Aortic Aneurysm. J Am Coll Cardiol. 2010;55:841–57.
4. Nienaber CA, Clough RE, Sakalihasan N, Suzuki T, Gibbs R, Mussa F, et al. Aortic dissection. Nat Rev Dis Primer. 2016;2:16053.
5. Pinard A, Jones GT, Milewicz DM. Genetics of Thoracic and Abdominal Aortic Diseases: Aneurysms, Dissections, and Ruptures. Circ Res. 2019;124:588–606.
6. Clough RE, Nienaber CA. Management of acute aortic syndrome. Nat Rev Cardiol. 2015;12:103–14.
7. Evangelista A, Isselbacher EM, Bossone E, Gleason TG, Eusanio MD, Sechtem U, et al. Insights From the International Registry of Acute Aortic Dissection: A 20-Year Experience of Collaborative Clinical Research. Circulation. 2018;137:1846–60.
8. Bossone E, Eagle KA. Epidemiology and management of aortic disease: aortic aneurysms and acute aortic syndromes. Nat Rev Cardiol. 2021;18:331–48.
9. Sherifova S, Holzapfel GA. Biomechanics of aortic wall failure with a focus on dissection and aneurysm: A review. Acta Biomater. 2019;99:1–17.
10. Beamish JA, He P, Kottke-Marchant K, Marchant RE. Molecular Regulation of Contractile Smooth Muscle Cell Phenotype: Implications for Vascular Tissue Engineering. Tissue Eng Part B Rev. 2010;16:467–91.
11. Chakraborty A, Li Y, Zhang C, Li Y, Rebello KR, Li S, et al. Epigenetic Induction of Smooth Muscle Cell Phenotypic Alterations in Aortic Aneurysms and Dissections. Circulation. 2023;148:959–77.
12. Luo Y, Luo J, An P, Zhao Y, Zhao W, Fang Z, et al. The activator protein-1 complex governs a vascular degenerative transcriptional programme in smooth muscle cells to trigger aortic dissection and rupture. Eur Heart J. 2024;45:287–305.
13. Liu R, Lo L, Lay AJ, Zhao Y, Ting KK, Robertson EN, et al. ARHGAP18 Protects Against Thoracic Aortic Aneurysm Formation by Mitigating the Synthetic and Proinflammatory Smooth Muscle Cell Phenotype. Circ Res. 2017;121:512–24.
14. Petsophonsakul P, Furmanik M, Forsythe R, Dweck M, Schurink GW, Natour E, et al. Role of Vascular Smooth Muscle Cell Phenotypic Switching and Calcification in Aortic Aneurysm Formation: Involvement of Vitamin K-Dependent Processes. Arterioscler Thromb Vasc Biol. 2019;39:1351–68.
15. Clément M, Chappell J, Raffort J, Lareyre F, Vandestienne M, Taylor AL, et al. Vascular Smooth Muscle Cell Plasticity and Autophagy in Dissecting Aortic Aneurysms. Arterioscler Thromb Vasc Biol. 2019;39:1149–59.
16. Nienaber CA, Clough RE. Management of acute aortic dissection. The Lancet. 2015;385:800–11.
17. Howard DPJ, Banerjee A, Fairhead JF, Perkins J, Silver LE, Rothwell PM. Population-Based Study of Incidence and Outcome of Acute Aortic Dissection and Premorbid Risk Factor Control.
18. Gao P, Gao P, Zhao J, Shan S, Luo W, Slivano OJ, et al. MKL1 cooperates with p38MAPK to promote vascular senescence, inflammation, and abdominal aortic aneurysm. Redox Biol. 2021;41:101903.
19. Liu Z-L, Li Y, Lin Y-J, Shi M-M, Fu M-X, Li Z-Q, et al. Aging aggravates aortic aneurysm and dissection via miR-1204-MYLK signaling axis in mice. Nat Commun. 2024;15:5985.
20. Lu H, Tian Z, Cui Y, Liu Z, Ma X. Chlorogenic acid: A comprehensive review of the dietary sources, processing effects, bioavailability, beneficial properties, mechanisms of action, and future directions. Compr Rev Food Sci Food Saf. 2020;19:3130–58.
21. Li L, Su C, Chen X, Wang Q, Jiao W, Luo H, et al. Chlorogenic Acids in Cardiovascular Disease: A Review of Dietary Consumption, Pharmacology, and Pharmacokinetics. J Agric Food Chem. 2020;68:6464–84.
22. He X, Wang C, Zhang Q, Yang T, Guo Q, Wang Y, et al. Identifying ENO1 as a protein target of chlorogenic acid to inhibit cellular senescence and prevent skin photoaging in mice. Aging Cell. 2024;e14433.
23. Suphakhong K, Terashima M, Wanna-udom S, Takatsuka R, Ishimura A, Takino T, et al. m6A RNA methylation regulates the transcription factors JUN and JUNB in TGF-β-induced epithelial–mesenchymal transition of lung cancer cells. J Biol Chem. 2022;298:102554.

24. Zhang Z, Li B, Xu P, Yang B. Integrated Whole Transcriptome Profiling and Bioinformatics Analysis for Revealing Regulatory Pathways Associated With Quercetin-Induced Apoptosis in HCT-116 Cells. Front Pharmacol. 2019;10:798.
25. Watson A, Nong Z, Yin H, O'Neil C, Fox S, Balint B, et al. Nicotinamide Phosphoribosyltransferase in Smooth Muscle Cells Maintains Genome Integrity, Resists Aortic Medial Degeneration, and Is Suppressed in Human Thoracic Aortic Aneurysm Disease. Circ Res. 2017;120:1889–902.
26. Franklin MK, Sawada H, Ito S, Howatt DA, Amioka N, Liang C-L, et al. β-Aminopropionitrile Induces Distinct Pathologies in the Ascending and Descending Thoracic Aortic Regions of Mice. Arterioscler Thromb Vasc Biol. 2024;44:1555–69.
27. Wu Q, O'Connor HM, Elston DM. Retrospective analysis of Verhoeff-Van Gieson elastic staining, diffractive microscopy, and Masson trichrome staining in the diagnosis of alopecia. J Am Acad Dermatol. 2020;82:247–9.
28. Dong W, Matsuno Y, Kameyama A. A Procedure for Alcian Blue Staining of Mucins on Polyvinylidene Difluoride Membranes. Anal Chem. 2012;84:8461–6.
29. Gao Y, Wu T, Tang X, Wen J, Zhang Y, Zhang J, et al. Increased cellular senescence in doxorubicin-induced murine ovarian injury: effect of senolytics. GeroScience. 2023;45:1775–90.
30. Yang K, Ren J, Li X, Wang Z, Xue L, Cui S, et al. Prevention of aortic dissection and aneurysm via an ALDH2-mediated switch in vascular smooth muscle cell phenotype. Eur Heart J. 2020;41:2442–53.
31. Ouyang Y, Hong Y, Mai C, Yang H, Wu Z, Gao X, et al. Transcriptome analysis reveals therapeutic potential of NAMPT in protecting against abdominal aortic aneurysm in human and mouse. Bioact Mater. 2024;34:17–36.
32. Zheng C, Zhong Y, Zhang W, Wang Z, Xiao H, Zhang W, et al. Chlorogenic Acid Ameliorates Post-Infectious Irritable Bowel Syndrome by Regulating Extracellular Vesicles of Gut Microbes. Adv Sci. 2023;10:2302798.
33. Naveed M, Hejazi V, Abbas M, Kamboh AA, Khan GJ, Shumzaid M, et al. Chlorogenic acid (CGA): A pharmacological review and call for further research. Biomed Pharmacother. 2018;97:67–74.
34. Surma S, Sahebkar A, Banach M. Coffee or tea: Anti-inflammatory properties in the context of atherosclerotic cardiovascular disease prevention. Pharmacol Res. 2023;187:106596.
35. Ontawong A, Duangjai A, Vaddhanaphuti CS, Amornlerdpison D, Pengnet S, Kamkaew N. Chlorogenic acid rich in coffee pulp extract suppresses inflammatory status by inhibiting the p38, MAPK, and NF-κB pathways. Heliyon. 2023;9:e13917.
36. Chen J, Zhou Z, Wu N, Li J, Xi N, Xu M, et al. Chlorogenic acid attenuates deoxynivalenol-induced apoptosis and pyroptosis in human keratinocytes via activating Nrf2/HO-1 and inhibiting MAPK/NF-κB/NLRP3 pathways. Biomed Pharmacother. 2024;170:116003.
37. Chen H-Z, Wang F, Gao P, Pei J-F, Liu Y, Xu T-T, et al. Age-Associated Sirtuin 1 Reduction in Vascular Smooth Muscle Links Vascular Senescence and Inflammation to Abdominal Aortic Aneurysm. Circ Res. 2016;119:1076–88.
38. Girsang E, Ginting CN, Lister INE, Gunawan KY, Widowati W. Anti-inflammatory and antiaging properties of chlorogenic acid on UV-induced fibroblast cell. PeerJ. 2021;9:e11419.
39. Yankova E, Blackaby W, Albertella M, Rak J, De Braekeleer E, Tsagkogeorga G, et al. Small-molecule inhibition of METTL3 as a strategy against myeloid leukaemia. Nature. 2021;593:597–601.
40. Exploration - 2024 - Xu - Exploring precision treatments in immune-mediated inflammatory diseases Harnessing the infinite.pdf.
41. Nabavi SF, Tejada S, Setzer WN, Gortzi O, Sureda A, Braidy N, et al. Chlorogenic Acid and Mental Diseases: From Chemistry to Medicine. Curr Neuropharmacol. 2017;15:471–9.
42. Amano Y, Honda H, Nukada Y, Ikeda N, Yamane M, Nakano K, et al. Safety Pharmacological Evaluation of the Coffee Component, Caffeoylquinic Acid, and Its Metabolites, Using Ex Vivo and In Vitro Profiling Assays. Pharmaceuticals. 2019;12:110.
43. Behne S, Franke H, Schwarz S, Lachenmeier DW. Risk Assessment of Chlorogenic and Isochlorogenic Acids in Coffee By-Products. Molecules. 2023;28:5540.
44. Tu, Y., Dai, G., Chen, Y., Tan, L., Liu, H. and Chen, M. (2025), Emerging Target Discovery Strategies Drive the Decoding of Therapeutic Power of Natural Products and Further Drug Development: A Case Study of Celastrol. Exploration e20240247. .